SARGENT & LUNDY
ENGINEERS
CHICAGO

Regulatory Docket File

STRESS ANALYSIS OF CRACKED PIPE JUNCTION IN DRESDEN-2 NUCLEAR POWER STATION

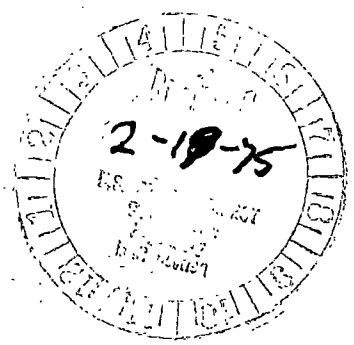

BY

ENGINEERING MECHANICS DIVISION
OF MECHANICAL DEPARTMENT

DECEMBER 4, 1974

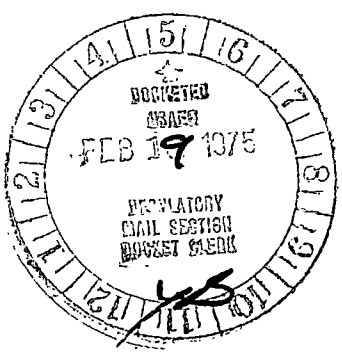

50-237/249
50-254/265

EMD File 5000-24

Regulatory Docket File

SARGENT & LUNDY
ENGINEERS
CHICAGO

STRESS ANALYSIS OF CRACKED PIPE JUNCTION IN DRESDEN-2 NUCLEAR POWER STATION

BY

ENGINEERING MECHANICS DIVISION
OF MECHANICAL DEPARTMENT

DECEMBER 4, 1974

EMD File 5000-24

SARGENT & LUNDY
ENGINEERS
CHICAGO

ANALYZED BY _____
V. K. Verma
Engineering Analyst

_____
J. W. Leonard
Consultant

REVIEWED BY _____
M. A. Salmon
Section Head

APPROVED BY _____
E. B. Branch
Division Head

APPROVED BY _____
F. L. Spakoski
Project Manager

SARGENT & LUNDY
ENGINEERS
CHICAGO

STRESS ANALYSIS OF CRACKED PIPE JUNCTION IN DRESDEN-2 NUCLEAR POWER STATION

REV.	REMARKS	DATE	APPROVAL
0	First Issue	December 4, 1974	EBB

TABLE OF CONTENTS

LIST OF TABLES

LIST OF FIGURES

SECTION 1. INTRODUCTION AND CONCLUSIONS

1.1 INTRODUCTION

A detailed stress analysis has been carried out for the 4 inch recirculation by-pass line pipe junction in the Dresden-2 Nuclear Power Station. This study was prompted by the detection of a crack in the recirculation discharge valve 4" by-pass, near the junction of that line with the 28" Loop B Recirculation line. Because subsequent examinations revealed similar cracking in the by-pass lines of Dresden-2, Loop A and Quad Cities-2, Loop B, it became necessary to determine, in detail, the magnitude of stresses in the neighborhood of the cracked junctions. This detailed analysis was used to verify the integrity of the junction from a stress analysis point of view and to provide stress intensity background information to supplement investigations of other potential causes for the crack occurrences.

The Dresden-2 Loop B crack was selected for analysis. A schematic view of the 4" by-pass line is shown in Figure 1. In that figure are shown the location of the crack in the 4" line and relative location of the crack zone within the cross-section of the pipe. The particular crack under investigation occurred just before the junction of the 4" line with the "weldolet" branch connection (Bonney Forge weldolet 28" x 4", extra strong TP 304) to the 28" main recirculation line. The crack zone approximately straddled

a radial line at 90° counter clockwise from the Y-axis of Figure 1. A schematic of the branch/weldolet/run pipe connection is shown in Figure 2. Also shown in Figure 2 is an enlarged photograph of the cracked section as obtained by Argonne Laboratories from a specimen cut from the 4" pipe. The geometric data used in the stress analysis was obtained from that specimen, and the ground-out section on the I.D. near the crack was included in the analytical model. The thicknesses at various locations along the specimen are given in Table 1.

The stress analysis was carried out using the finite element method with a standard computer program and is described in Section 2 of this report. The numerical results of the stress analysis for various combinations of loadings are given in Section 3. The interpretation of those numerical results are contained in Section 3 along with conclusions on the influence of stress intensities on the occurrence of the crack.

1.2 CONCLUSIONS

1. All stresses due to the loading conditions imposed in the analysis were well below typical design code allowables.
2. For the local weldolet pipe region studied, the maximum stressed section was not the section where the crack occurred. The maximum stress section was found to be the section between the weld and the weldolet.
3. Within the crack zone section the maximum stress did occur near the crack zone.

SECTION 2. ANALYSIS METHOD

It was decided to perform a finite element analysis of the weldolet to pipe junction in order to determine the distribution of stress at critical cross-sections of the pipe. The finite element method is a numerical modelling technique by which a continuum can be approximated by a finite number of elements. The elements retain the elastic properties of the continuum. Solutions within each of the elements are postulated and expressed in terms of a discrete number of unknown parameters at the nodal points of the elements. By interconnection of the elements at the nodal points, a set of algebraic equations is generated in terms of the unknown parameters. Then, the solution to the simultaneous algebraic equations is used to determine the stress characteristics within each element.

The pipe junction can be modelled geometrically as a collection of axisymmetric ring elements, each ring having a triangular or quadrilateral cross-section as shown in Figure 3. The longitudinal axis of the 4" by-pass pipe was taken as the axis of symmetry. The mesh of 500 elements and 548 nodes used to model the junction is also shown in Figure 3. It can be seen that a graded mesh was used with small elements assumed in the immediate area of the observed crack location.

For analysis purposes it was necessary to isolate the junction from the rest of the piping system. This was done by passing imaginary sections through the junction at points A and B in Figure 3. At section A, it was assumed that the 28" pipe constrained the junction from both radial and axial motion and was therefore idealized as a completely fixed section. At section B, the pipe was unconstrained against both radial and axial motion. The effect of the internal stresses at section B was replaced by edge loads on the finite element model at section B. The magnitude of the edge loads will be detailed subsequently when the various load cases considered are discussed. The axial location of section B was taken as 5.833" from section A. This is sufficient distance (1)* to insure that the localized distorsions due to the edge load idealization will have no effect on the calculated stress distributions at the crack location.

The computer program used for the analysis is entitled ASAL (Finite Element Analysis of Axisymmetric Solids With Arbitrary Loadings) (2). In the program, axisymmetric solid quadrilateral or triangular elements are used to model the goemetry of the structure. Each element may have different axisymmetric elastic properties. The loading

---

* Numbers in parentheses denote entries in Appendix A: References.

need not be axially symmetric. Applied loads, be they traction or nodal loads, are decomposed into Fourier harmonics. The response of the structure to each Fourier harmonic is determined, and the total response is then calculated by summation of the harmonics.

Input consists of problem identification and control information, material characterization, nodal point identification with boundary conditions, element identification and Fourier information.

Output is in the form of nodal point displacements and element stresses for each Fourier term, that is the three displacement components and six components of stresses and strains. A summation of stresses and displacements also may be obtained at specified circumferential angles.

The material properties assumed (3) for the various components of the pipe junction and given in Table 2.

Four basic load conditions were considered in the analysis.

1) pressure loading
2) dead weight loading due to 4" pipe and valve
3) thermal expansion loading with 4" and 28" line hot
4) thermal expansion loading with 4" line cold and 28" line hot.

Various combinations of these load conditions were also considered in order to determine the maximum stress combination.

The magnitude of pressure and of end-section loads are displayed in Table 3 for each load condition. The location of end-section load application and definition of sign convention is shown in Figure 4(a). The local coordinate axes are also defined in Figure 1.

For load condition 5, the stresses due to thermal transients during start up were determined and incorporated in the analysis along with the end-section loads. It was assumed that the temperature of the 28" main line increased from 150°F to 540°F in eight hours, while the temperature of the 4" line away from the junction was held at 150°F. The transient temperature gradients along the 4" line during this period were found by numerical analysis (4). The steepest gradient occurred 7½ hours after start up. This temperature distribution, shown in Figure 4(b) was input as nodal point temperature to the ASAL Program for calculation of the induced thermal stresses.

The different load components given in Table 3 for the various loading condition were used to determine the appropriate input loads for the ASAL Program.

Pressure Load - A uniform normal traction of 1050 psi was applied to each element along the interior of pipe. In addition, the F_x force was modelled by applying axially uniform tractions $F_x/\pi(R_o^2-R_i^2)$ to the two end elements at section B in Figure 5a, where R_o = outer radius and

R_i = inner radius of 4" pipe. The pressure and F_x tractions were treated as zero-harmonic (symmetric) terms in the Fourier analysis.

End-Section Torsion Loading - The torsional moments M_x were modelled as axially symmetric loads applied to the nodes at section B in Figure 5(b). They were input as circumferentially directed loads with magnitudes of $M_x/\pi(R_o+R_i)$ pounds per radian. They were treated as zero harmonic (symmetric) terms in the Fourier analysis.

End-Section Moment Loads - The moments M_y and M_z were combined to obtain a resultant normal moment $M_r = \sqrt{M_y^2+M_z^2}$ applied at a clockwise circumferential angle $\theta_r = \tan^{-1}(M_y/M_z)$ with the z-axis. A shift in the angular origin of amount θ_r was performed (See Figure 6). The moment resultant M_r was modelled by calculating the equivalent normal axial traction on each element of section B in Figure 6 as

$$\sigma_{b1} = \frac{M_r\, \eta_1}{I} \qquad \sigma_{b2} = \frac{M_r\, \eta_2}{I}$$

where

σ_{bi} = uniform traction on element i in Figure 6
I = moment of inertia of pipe
$\eta_1 = R_i + 1/4\ (R_o - R_i)\ \cos\theta$
$\eta_2 = R_i + 3/4\ (R_o - R_i)\ \cos\theta$
θ = circumferential angle from new axis

These tractions were applied as first harmonic (cos θ) terms in the Fourier analysis.

Numeric results for stress in the junction are given in

the next section for various combinations of the basic load conditions listed in Table 3.

SECTION 3. NUMERICAL RESULTS AND INTERPRETATION

In this section are presented the stress distributions at the two critical cross-sections of the pipe junction; those cross-sections being located at the crack zone section (Section 1) and at the pipe to weldolet section (Section 2) respectively. (See Figure 3)

Combinations of the loading conditions tabulated in Table 3 were considered in order to arrive at the worst loading combination. The "worst loading" combination was defined as that combination of loading cases which produces maximum longitudinal and circumferential stresses in the junction.

For convenience, the loading conditions of Table 3 were separated into the following load cases for application of the finite element method. For the cases selected maximum stresses at the critical cross-sections are given in Tables 4 through 8.

Load Cases

1) Pressure loading (condition 1)

2) Torsion loading for dead weight plus thermal (28" HOT - 4" COLD) load. (condition 2 plus 4)

3) Moment loading for dead weight only (condition 2)

4) Moment loading for dead weight plus thermal (28" HOT - 4" COLD) load. (condition 2 plus 4)

5) Thermal gradient loading only. (condition 5)

The distribution of longitudinal and circumferential stresses

through the thickness for each of these load cases are plotted in Figures 7 to 11. The worst loading combination was found to be a summation of cases 1, 2, 4, and 5 given above. The maximum stresses for this combination are given in Table 9 and, the distributions through the thickness are plotted in Figure 12. Tables 6 and 7 also give the stress components at the approximate center of the crack zone (see Figure 6). In Table 10 the principal stresses and stress intensities at the two critical sections and also at the approximate center of the crack zone are given for the "worst loading combination".

From Table 10, it can be seen that the maximum stress state occurred at the weld-to-weldolet section rather than at the crack zone section. However, at the crack zone section, the maximum stresses occurred at 105.8° counter clockwise from the Y-axis which is very near the center of the crack zone.

For the worst case combination, the radial stress component never exceeds 1600 psi in absolute value. The absolute value of the axial stress never exceeds 9700 psi except near the outer edge of the weld-to-weldolet section where it equals 19700 psi. Similarly, the circumferential stress never exceeds 8300 psi except near the outer edge of the weld-to-weldolet section where it equals 11203 psi. Shear stresses throughout the junction are negligible i.e., less than 1500 psi. The reason for the large stress at the outer edge of the weld-to-weldolet section is that this is a point of stress concentration caused

by the discontinuity in sectional geometry. This stress riser effect is highly localized in nature as can be seen in Figure 12.

The principal stresses and stress intensities in Table 10 can be summarized as follows:

1) at the crack zone section, the maximum principal stress equals 9837 psi and maximum stress intensity equals 10107 psi;

2) in the approximate crack zone location (90° counter clockwise from Y-axis) in the cracked section, the maximum principal stress equals 9630 psi, and the maximum stress intensity equals 9911 psi; and

3) at the weld-to-weldolet section: the maximum principal stress was everywhere less than 10212 psi (stress intensity less than 9300 psi) except near the outer edge where the maximum principal stress equals 19967 psi and the maximum stress intensity equals 18466 psi.

The yield stress of the weldolet and the pipe material is approximately 18800 psi at 550°F and the yield stress of the weld material is in the range 30-35000 psi at 550°F. At the crack zone section the stress intensity does not exceed 54% of the yield stress for the pipe. The same is true at the weld-to-weldolet section, except for the stress concentration at the outer edge.

The "worst combination" maximum intensities of Table 10 are well within the ASME Section III stress criteria of 3 Sm for the combination of primary plus secondary stresses. Sm for the pipe material at 550°F is 16900 psi, and 3 Sm is 50700 psi.

TABLE 1 - THICKNESS MEASUREMENTS IN THE VICINITY OF CRACK

SECTION *	THICKNESS (inches)
1	.3814
2	.3888
3	.3890
4	.3658
5	.3462
6	.4983
7	.5158
8	.5078

* Sections number are shown in Figure 2.

TABLE 2. MATERIAL PROPERTIES

Component	4" Pipe	Weld	Weldolet
Material Designation	TP304	TP309	TP304
Youngs Modulus (psi)	$28X10^6$	$29X10^6$	$28X10^6$
Poisson's ratio	0.3	0.3	0.3
Coefficient of thermal expansion (in/in/°F)	$9.9X10^{-6}$	$9.9X10^{-6}$	$9.9X10^{-6}$
Yield stress (psi) at 550°F	$18.8X10^3$	$30-35X10^3$	$20X10^3$

TABLE 3. BASIC LOAD CONDITIONS *

No.	Load Condition	Pressure (psi)	M_x (in-lbs)	M_y (in-lbs)	M_z (in-lbs)	F_x (lbs)	F_y (lbs)	F_z (lbs)
1.	Pressure	1050	-	-	-	12071.7	-	-
2.	Weight of 4" pipe and valve	-	-616	-2160	-7580	-18.6	-159.8	91.25
3.	Thermal expansion 28" HOT (546F) - 4" HOT (546F)	-	12	-867	-215	-4.86	-16.76	36.74
4.	Thermal expansion 28" HOT (546F) - 4" COLD (150F)	-	10418.9	29767.3	15379.5	-76.6	369.9	-676.9
5.	Transient thermal gradient	-	-	-	-	-	-	-

* Loads Obtained From General Electric on 9-26-74. Sign Convention for Forces and Moments Shown on Figures 1 and 4(a). Loads are Acting on Weldolet From the 4 inch Pipe.

TABLE 4 STRESS COMPONENTS AT CRITICAL SECTIONS DUE TO LOAD CASE 1.

SECTION NUMBER	r-coordinate	σ_{rr} (Radial)	σ_{zz} (Axial)	σ_{tt} (Hoop)	σ_{rz}	σ_{zt}	σ_{rt}
1 (all θ)	1.99	-947.1	2532	5900	-70.25	0.0	0.0
	2.02	-758.3	2547	5898	-105.5	0.0	0.0
	2.06	-590.3	2586	5825	-134.5	0.0	0.0
	2.09	-442.6	2651	5760	-162.8	0.0	0.0
	2.12	-315.2	2746	5704	-192.1	0.0	0.0
	2.15	-209.6	2873	5656	-220.7	0.0	0.0
	2.19	-129.8	3037	5616	-242.1	0.0	0.0
	2.22	-81.9	3234	5579	-239.2	0.0	0.0
	2.25	-57.09	3440	5542	-186.8	0.0	0.0
	2.28	-27.21	3599	5495	-71.92	0.0	0.0
2 (all θ)	1.96	-998.8	297.1	4673	16.82	0.0	0.0
	2.00	-844.6	820.6	4659	-24.56	0.0	0.0
	2.05	-690.2	860.3	4612	-85.56	0.0	0.0
	2.09	-512.5	1318	4609	-121.5	0.0	0.0
	2.14	-345.6	1375	4582	-184.8	0.0	0.0
	2.18	-162.9	1847	4607	-207.1	0.0	0.0
	2.23	-10.73	1913	4588	-280.7	0.0	0.0
	2.27	+154.2	2689	4716	-239.5	0.0	0.0
	2.32	+213.7	2717	4665	-293.9	0.0	0.0
	2.36	+441.2	5605	5449	+446.4	0.0	0.0

All Stresses in psi. A Positive Normal Stress Denotes Tension

TABLE 5 STRESS COMPONENTS AT CRITICAL SECTION DUE TO LOAD CASE 2.

SECTION NUMBER	r-coordinate	σ_{rr} (Radial)	σ_{zz} (Axial)	σ_{tt} (Hoop)	σ_{rz}	σ_{zz}	σ_{rt}
	1.99	0.0	0.0	0.0	0.0	996	-16.9
	2.02	0.0	0.0	0.0	0.0	993	-24.1
	2.06	0.0	0.0	0.0	0.0	996	-30.7
	2.09	0.0	0.0	0.0	0.0	1000	-36.1
1	2.12	0.0	0.0	0.0	0.0	1020	-41.3
(all θ)	2.15	0.0	0.0	0.0	0.0	1030	-44.1
	2.19	0.0	0.0	0.0	0.0	1060	-43.9
	2.22	0.0	0.0	0.0	0.0	1080	-39.1
	2.25	0.0	0.0	0.0	0.0	1110	-27.7
	2.28	0.0	0.0	0.0	0.0	1130	-10.2
	1.96	0.0	0.0	0.0	0.0	586	-6.79
	2.00	0.0	0.0	0.0	0.0	616	-11.1
	2.05	0.0	0.0	0.0	0.0	616	-20.0
	2.09	0.0	0.0	0.0	0.0	663	-22.9
2	2.14	0.0	0.0	0.0	0.0	664	-31.5
(all θ)	2.18	0.0	0.0	0.0	0.0	734	-27.2
	2.23	0.0	0.0	0.0	0.0	735	-31.3
	2.27	0.0	0.0	0.0	0.0	862	-0.7
	2.32	0.0	0.0	0.0	0.0	858	+17.6
	2.36	0.0	0.0	0.0	0.0	1180	156.0

All Stresses in psi. A Positive Normal Stress Denotes Tension

TABLE 6 STRESS COMPONENTS AT CRITICAL SECTIONS DUE TO LOAD CASE 3.

SECTION NUMBER	R-COORDINATE	σ_{rr} (Radial)	σ_{zz} (Axial)	σ_{tt} (Hoop)	σ_{rz}	σ_{zt}	σ_{rt}
1 (15.9° clockwise from Y-axis, Fig. 1)	1.99	23.75	1734	340.5	-37.18	0.0	0.0
	2.02	60.90	1670	323.3	-58.22	0.0	0.0
	2.06	85.91	1627	310.1	-74.97	0.0	0.0
	2.09	100.8	1605	300.5	-90.38	0.0	0.0
	2.12	106.7	1600	294.1	-105.4	0.0	0.0
	2.15	103.5	1612	290.2	-119.2	0.0	0.0
	2.19	89.99	1642	288.2	-128.4	0.0	0.0
	2.22	63.87	1685	286.0	-124.6	0.0	0.0
	2.25	30.53	1727	280.8	-95.76	0.0	0.0
	2.28	4.9	1738	268.3	-36.34	0.0	0.0
1 (90° Counter Clockwise from Y-axis, Fig. 1)	1.99	-6.51	-475.0	-93.27	10.19	-65.72	2.70
	2.02	-16.68	-457.4	-88.57	15.95	-69.26	5.66
	2.06	-23.54	-445.8	-84.96	20.54	-72.91	7.59
	2.09	-27.63	-439.6	-82.34	24.76	-76.73	8.72
	2.12	-29.24	-438.3	-80.56	28.87	-80.80	9.18
	2.15	-28.36	-441.7	-79.49	32.65	-85.17	9.06
	2.19	-24.65	-449.9	-78.95	35.19	-89.90	8.37
	2.22	-17.50	-461.6	-78.35	34.15	-95.03	7.04
	2.25	+8.36	-473.1	-76.93	26.24	-100.6	4.92
	2.28	+1.34	-476.3	-73.51	9.96	-106.5	1.88
2 (15.9° clockwise from Y-axis, Fig. 1)	1.96	-7.16	350.5	173.1	-11.58	0.0	0.0
	2.00	8.64	601.0	246.8	-36.32	0.0	0.0
	2.05	31.83	616.8	254.2	-83.45	0.0	0.0
	2.09	66.60	830.7	320.9	-102.6	0.0	0.0
	2.14	101.4	855.8	334.2	-144.3	0.0	0.0
	2.18	142.9	1079	405.8	-154.0	0.0	0.0
	2.23	172.8	1108	418.4	-194.9	0.0	0.0
	2.27	206.2	1494	536.0	-167.6	0.0	0.0
	2.32	189.3	1498	525.9	-190.3	0.0	0.0
	2.36	262.9	2988	980.0	209.8	0.0	0.0

All Stresses in psi. A Positive Normal Stress Denotes Tension

TABLE 7 STRESS COMPONENTS AT CRITICAL SECTIONS DUE TO LOAD CASE 4

SECTION NUMBER	r-coordinate	σ_{rr} (Radial)	σ_{zz} (Axial)	σ_{tt} (Hoop)	σ_{rz}	σ_{zt}	σ_{rt}
1 (105.8° counter clockwise from Y-axis, Fig. 1)	1.99	86.46	6311	1239	-135.3	0.0	0.0
	2.02	221.6	6077	1177	-211.9	0.0	0.0
	2.06	312.7	5923	1129	-272.8	0.0	0.0
	2.09	367.0	5840	1094	-328.9	0.0	0.0
	2.12	388.4	5823	1070	-383.5	0.0	0.0
	2.15	376.8	5869	1056	-433.8	0.0	0.0
	2.19	327.5	5977	1049	-467.5	0.0	0.0
	2.22	232.5	6132	1041	-453.7	0.0	0.0
	2.25	111.1	6285	1022	-348.5	0.0	0.0
	2.28	17.85	6327	976.6	-132.3	0.0	0.0
1 (90° counter clockwise from Y-axis, Fig. 1)	1.99	83.20	6073	1192	-130.2	67.61	-2.8
	2.02	213.3	5848	1132	-203.9	71.26	-5.8
	2.06	300.0	5700	1086	-262.6	75.01	-7.8
	2.09	353.2	5620	1053	-316.5	78.94	-9.0
	2.12	373.8	5604	1030	-369.1	83.13	-9.5
	2.15	362.6	5648	1016	-417.4	87.63	-9.3
	2.19	315.2	5752	1009	-449.9	92.49	-8.6
	2.22	223.7	5901	1002	-436.6	97.77	-7.2
	2.25	106.9	6048	983.5	-335.4	103.5	-5.1
	2.28	17.18	6089	939.8	-127.3	109.5	-1.9
2 (105.8° counter clockwise from Y-axis, Fig. 1)	1.96	-26.07	1276	630.1	-42.15	0.0	0.0
	2.00	31.44	2190	898.2	-132.2	0.0	0.0
	2.05	115.9	2245	925.1	-303.7	0.0	0.0
	2.09	242.4	3024	1168	-373.4	0.0	0.0
	2.14	369.1	3115	1216	-525.3	0.0	0.0
	2.18	520.1	3928	1477	-560.5	0.0	0.0
	2.23	629.1	4031	1523	-709.2	0.0	0.0
	2.27	750.6	5436	1951	-610.1	0.0	0.0
	2.32	689.0	5452	1914	-692.8	0.0	0.0
	2.36	956.7	10870	3567	763.4	0.0	0.0

All Stresses in psi. A Positive Normal Stress Denotes Tension

TABLE 8 STRESS COMPONENTS AT CRITICAL SECTIONS DUE TO LOAD CASE 5

SECTION NUMBER	r-coordinate	σ_{rr} (Radial)	σ_{zz} (Axial)	σ_{tt} (Hoop)	σ_{rz}	σ_{zt}	σ_{rt}
	1.99	8.28	160.5	694.9	-47.64	0.0	0.0
	2.02	21.63	96.04	665.6	-115.0	0.0	0.0
	2.06	26.88	44.09	638.5	-159.2	0.0	0.0
	2.09	27.39	-0.16	613.2	-186.0	0.0	0.0
1	2.12	22.36	-38.72	588.5	-197.7	0.0	0.0
(all θ)	2.15	17.75	-71.87	566.2	-195.5	0.0	0.0
	2.19	10.85	-104.8	543.7	-179.7	0.0	0.0
	2.22	3.57	-138.3	521.3	-148.3	0.0	0.0
	2.25	-3.15	-180.3	497.1	-100.8	0.0	0.0
	2.28	-2.62	-238.6	470.7	-37.18	0.0	0.0
	1.96	-136.7	-2280	706.0	-19.29	0.0	0.0
	2.00	-108.9	-1508	915.7	-198.1	0.0	0.0
	2.05	-60.58	-1485	917.6	-261.5	0.0	0.0
	2.09	+0.90	-746.3	1125	-400.5	0.0	0.0
2	2.14	59.46	-723.1	1129	-419.3	0.0	0.0
(all θ)	2.18	110.5	39.39	1340	-509.6	0.0	0.0
	2.23	147.6	43.78	1330	-501.5	0.0	0.0
	2.27	156.5	1066	1603	-501.3	0.0	0.0
	2.32	119.8	996	1547	-421.0	0.0	0.0
	2.36	179.4	3230	2187	+56.48	0.0	0.0

All Stresses in psi. A Positive Normal Stress Denotes Tension

TABLE 9 STRESS COMPONENTS AT CRITICAL SECTIONS DUE TO "WORST LOADING COMBINATION" (SUMMATION CASE 1, 2, 4 and 5)

SECTION NUMBER	r-coordinate	σ_{rr} (Radial)	σ_{zz} (Axial)	σ_{tt} (Hoop)	σ_{rz}	σ_{zt}	σ_{rt}
1 (105.8° counter clockwise from Y-axis, Fig. 1)	1.99	-852.4	9003	7914	-253.2	996	-16.9
	2.02	-515.1	8720	7741	-432.4	993	-24.1
	2.06	-250.7	8553	7593	-566.5	996	-30.7
	2.09	-48.21	8491	7467	-677.7	1000	-36.1
	2.12	+95.56	8530	7363	-773.3	1020	-41.3
	2.15	185.9	8670	7278	-850.0	1030	-44.1
	2.19	208.5	8909	7209	-889.3	1060	-43.9
	2.22	154.2	9228	7141	-841.2	1080	-39.1
	2.25	50.86	9545	7061	-636.1	1110	-27.7
	2.28	-11.98	9687	6942	-241.4	1130	-10.2
1 (90° counter clockwise from Y-axis, Fig. 1)	1.99	-855.6	8765	7866	-248.1	1064	-19.7
	2.02	-523.4	8491	7696	-424.4	1064	-29.9
	2.06	-262.5	8330	7549	-556.3	1071	-38.5
	2.09	-62.01	8271	7426	-665.3	1079	-45.0
	2.12	+80.96	8311	7323	-758.9	1103	-50.7
	2.15	170.75	8449	7238	-833.6	1118	-53.4
	2.19	196.25	8684	7169	-871.7	1153	-52.5
	2.22	145.4	8997	7102	-824.1	1178	-46.3
	2.25	46.66	9308	7023	-623.0	1214	-32.7
	2.28	-12.65	9449	6906	-236.4	1240	-12.1
2 (105.8° counter clockwise from Y-axis, Fig. 1)	1.96	-1162	-706.9	6009	-44.62	586	-6.8
	2.00	-922.1	+1503	6473	-354.9	616	-11.1
	2.05	-634.9	1620	6455	-650.8	616	-20.0
	2.09	-269.2	3596	6902	-895.4	663	-22.9
	2.14	+82.9	3767	6927	-1129	664	-31.5
	2.18	467.7	5814	7422	-1277	734	-27.2
	2.23	766.0	5988	7441	-1491	735	-31.3
	2.27	1061	9191	8270	-1351	862	-0.7
	2.32	1022	9165	8126	-1408	858	+17.6
	2.36	1577	19705	11203	+1266	1180	156.0

All Stresses in psi. A Positive Normal Stress Denotes Tension

TABLE 10 PRINCIIAL STRESSES AND STRESS INTENSITIES AT CRITICAL SECTIONS DUE TO "WORST LOADING COMBINATION" (SUMMATION OF CASE 1, 2, 4 and 5)

SECTION NUMBER	r-coordinate	Principal Stresses			Stress Intensities		
		σ_{max}	σ_{int}	σ_{min}	S_{max}	S_{int}	S_{min}
	1.99	9155	7862	-952	10107	8814	1293
	2.02	8977	7589	-621	9598	8210	1338
1	2.06	8908	7349	-362	9270	7711	1559
	2.09	8922	7152	-164	9086	7316	1770
(105.8° counter	2.12	9013	7001	-26	9039	7027	2012
clockwise	2.15	9174	6898	+61	9113	6837	2276
from	2.19	9397	6849	81	9316	6768	2548
Y-axis,	2.22	9637	6859	27	9610	6832	2778
Fig. 1)	2.25	9819	6915	-77	9897	6993	2904
	2.28	9837	6922	-142	9979	7064	2915
	1.99	8939	7808	-972	9911	8780	1131
	2.02	8781	7529	-647	9429	8177	1252
1	2.06	8725	7286	-394	9119	7680	1439
	2.09	8745	7090	-200	8944	7290	1654
(90° counter	2.12	8837	6942	-65	8902	7007	1895
clockwise	2.15	8993	6843	+22	8971	6821	2150
from	2.19	9210	6798	42	9168	6756	2412
Y-axis,	2.22	9441	6813	-92	9450	6822	2628
Fig. 1)	2.25	9614	6874	-110	9724	6984	2740
	2.28	9630	6885	-173	9802	7058	2745
	1.96	6009	-306	-1563	7572	6315	1257
	2.00	6499	1625	-1070	7569	4873	2696
2	2.05	6542	1693	-795	7337	4849	2488
	2.09	7134	3477	-382	7516	3859	3657
(105.8° counter	2.14	7297	3517	-371	7334	3780	3554
clockwise	2.18	8146	5192	+366	7781	4826	2954
from	2.23	8396	5139	660	7737	4479	3258
Y-axis,	2.27	10212	7342	968	9244	6374	2870
Fig. 1)	2.32	10199	7185	929	9270	6256	3014
	2.36	19967	11018	1500	18466	9518	8948

All Stresses in psi.

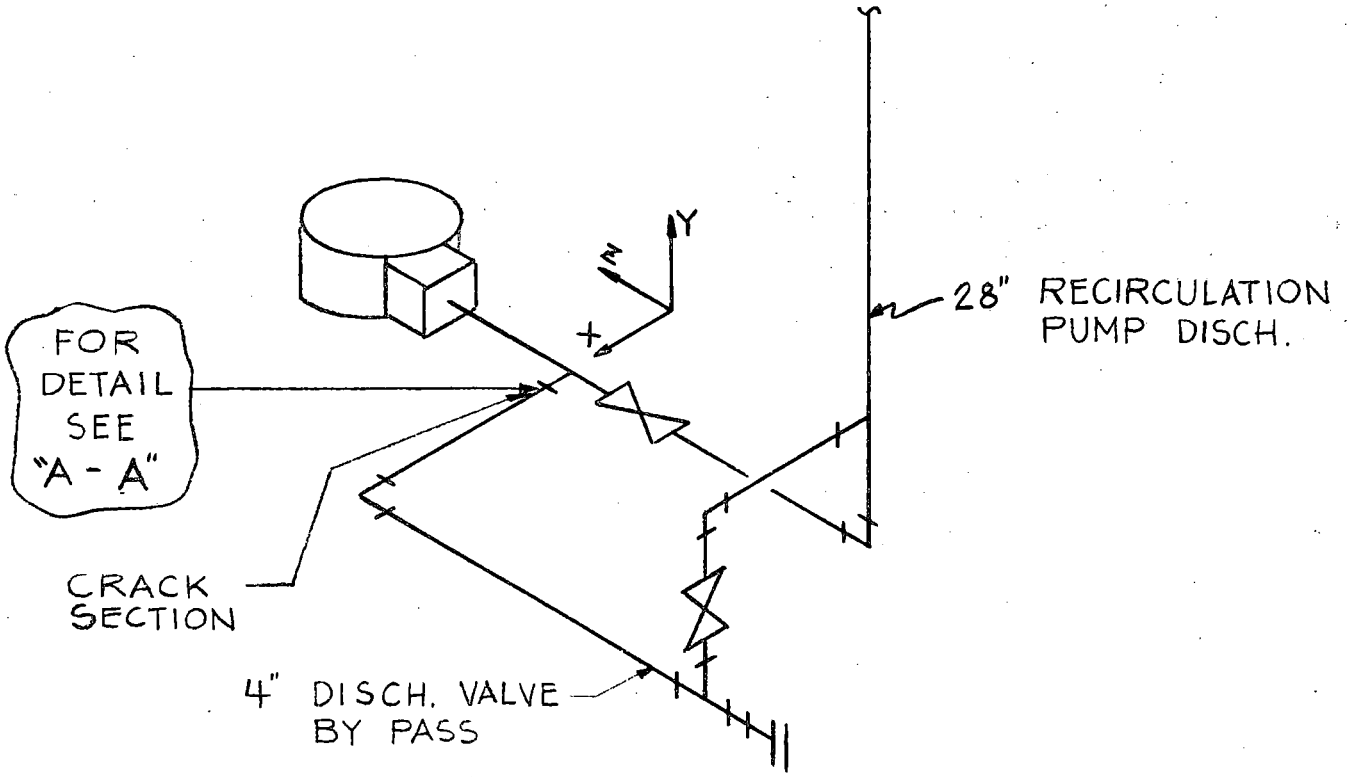

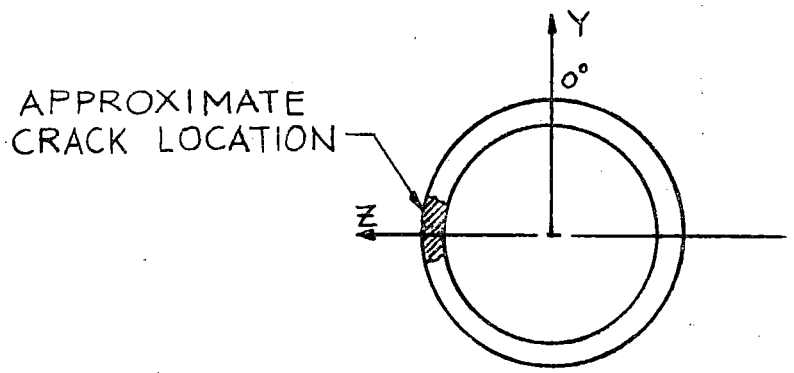

"A - A"
LOOKING AT
28" PIPE

Figure 1 Recirculation Loop B

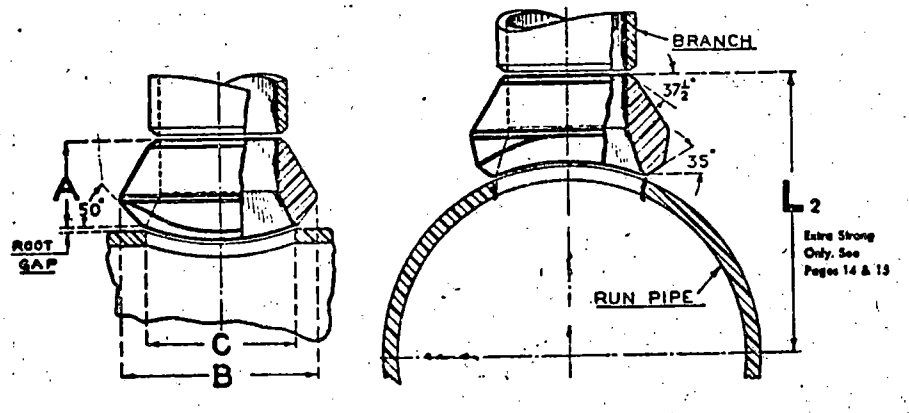

A = 2 inches
B = 6 inches
C = 4.75 inches

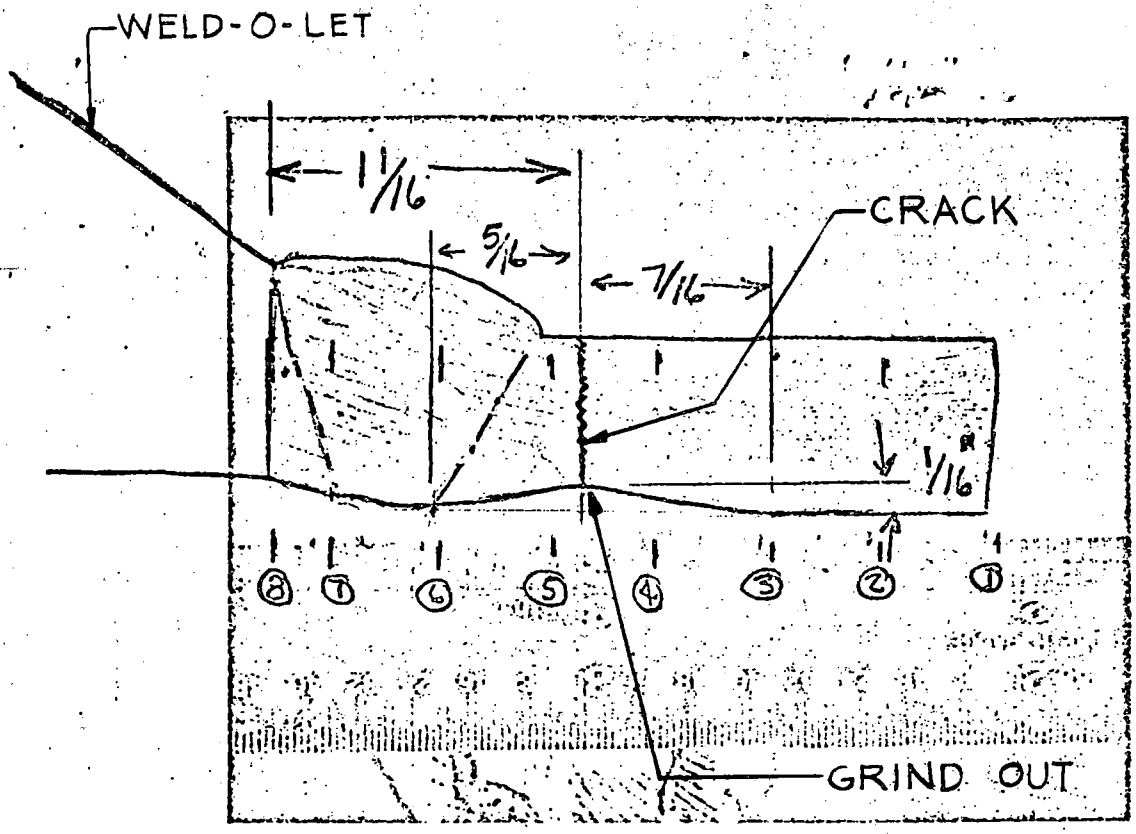

Figure 2 Branch/Weldolet/Run Pipe Connection

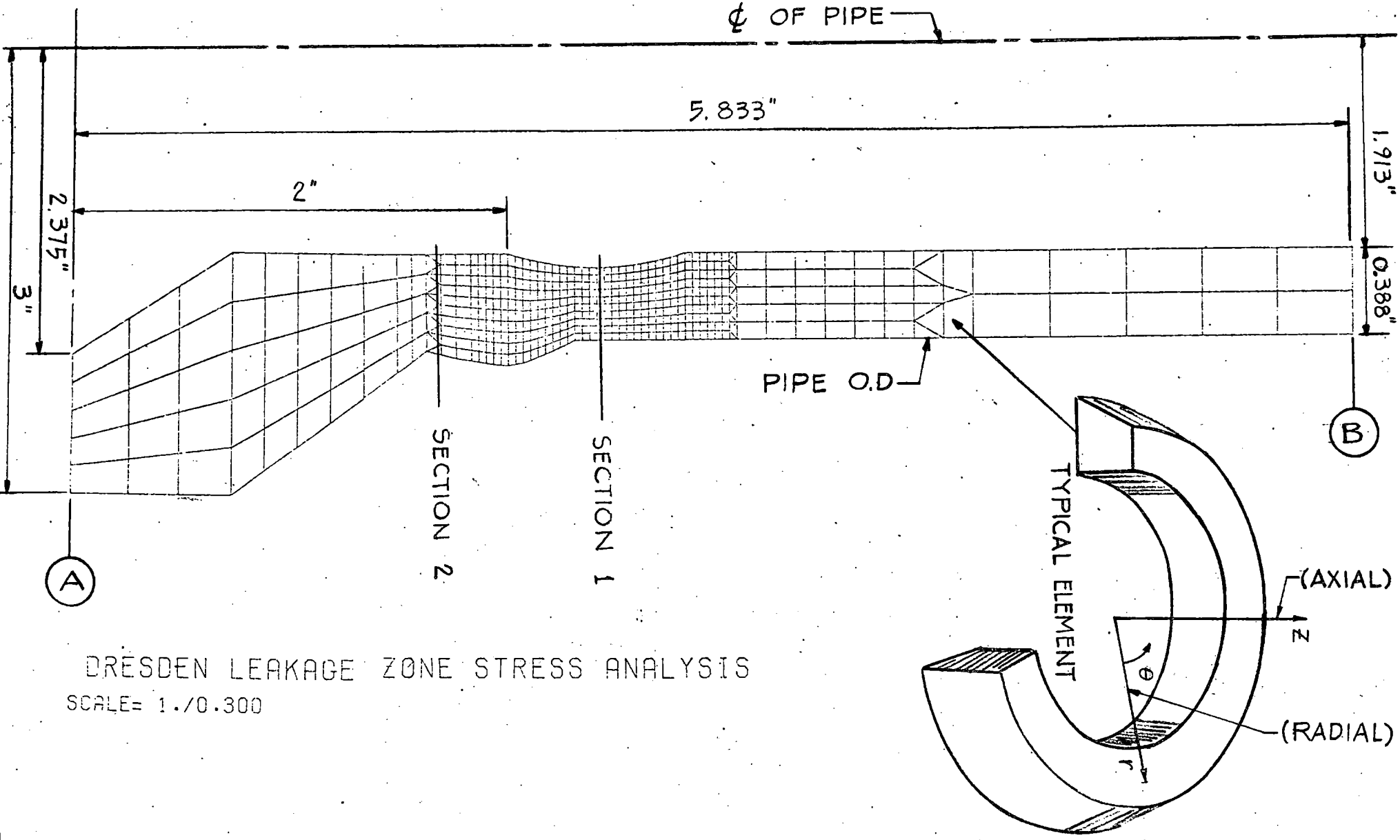

Figure 3 Finite Element Mesh and Typical Element

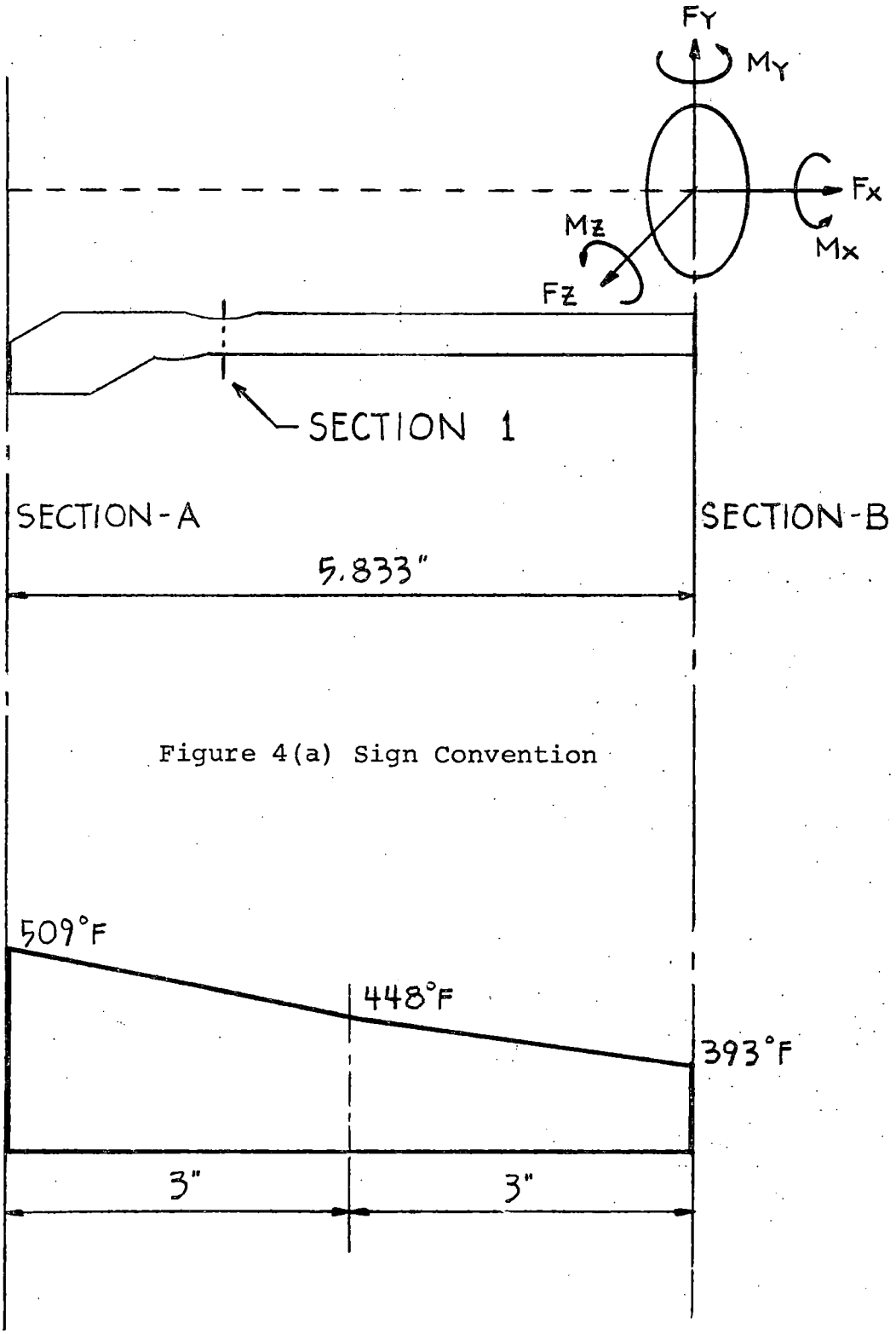

Figure 4(a) Sign Convention

Figure 4 (b) Transient Temperature Distribution @ Time 7½ Hours

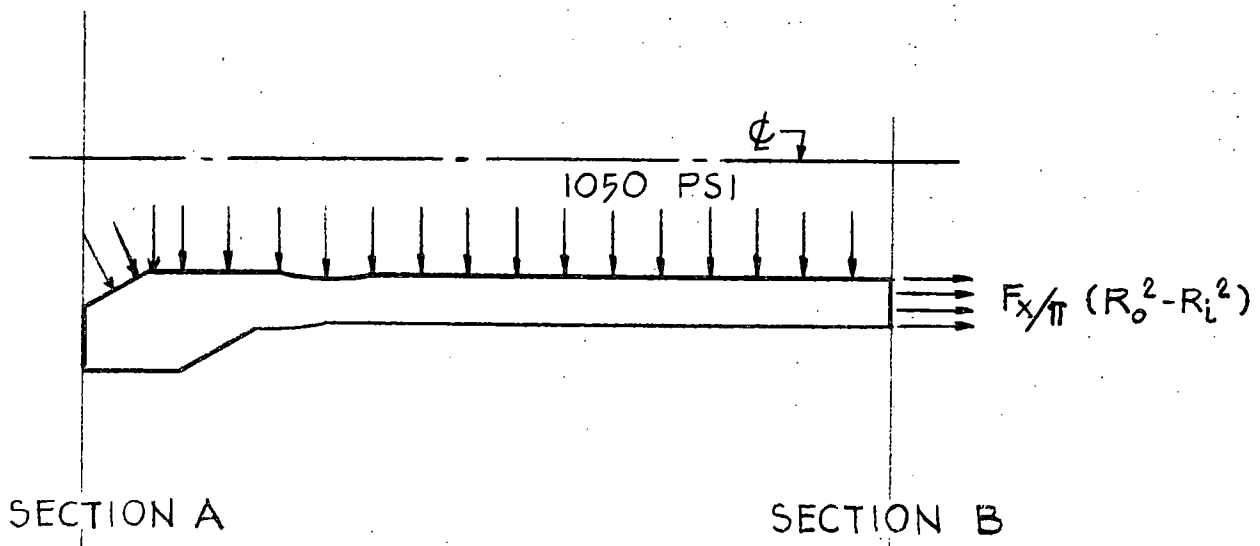

Figure 5(a) Pressure Loading Model

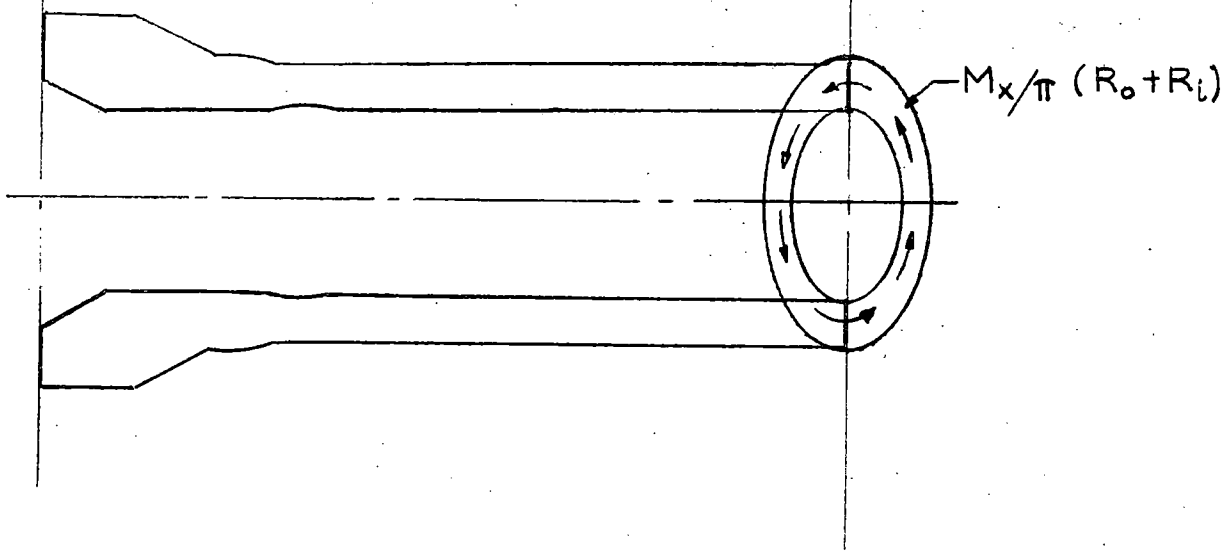

Figure 5 (b) Torsion Loading Model

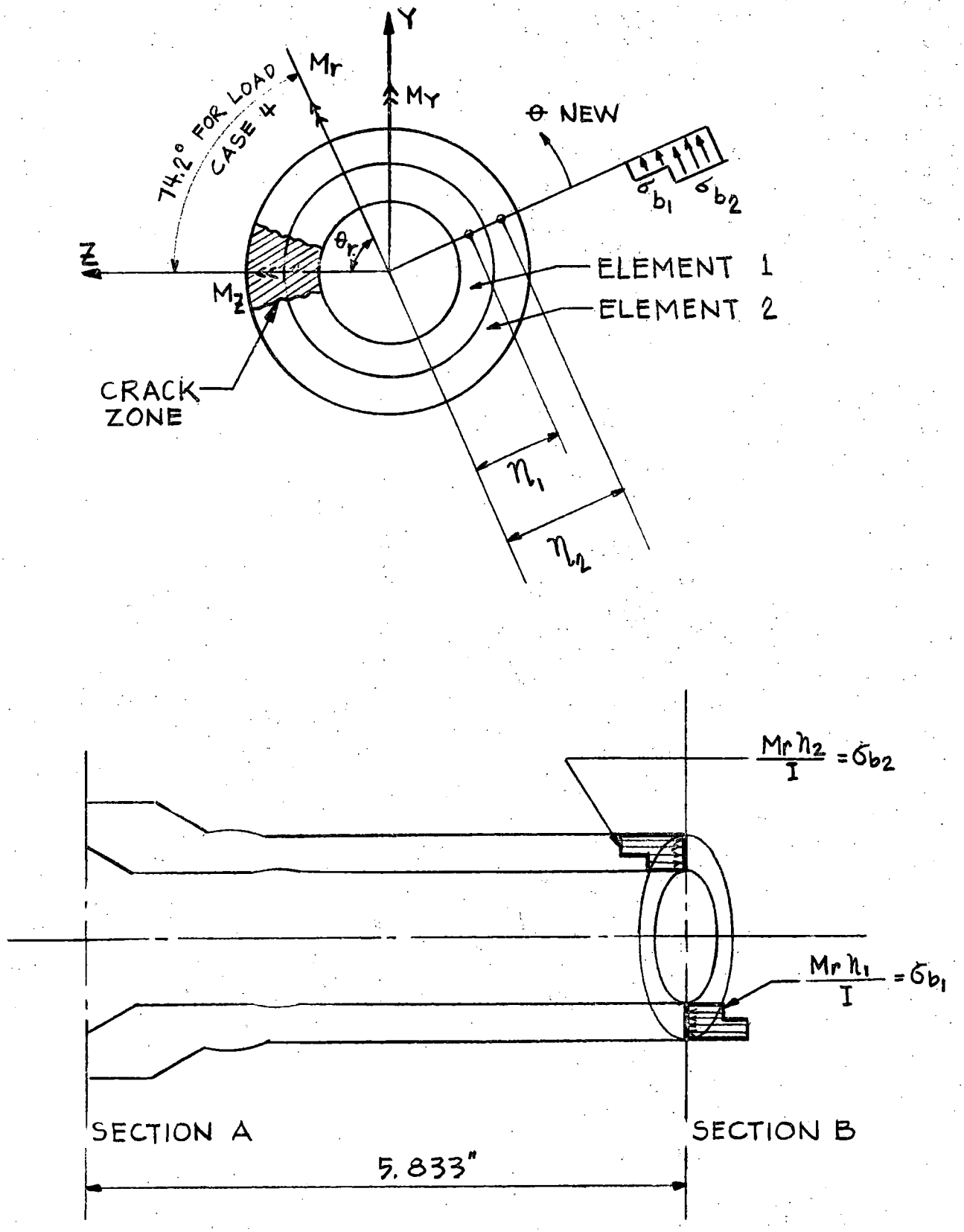

Figure 6 Moment Loading Model

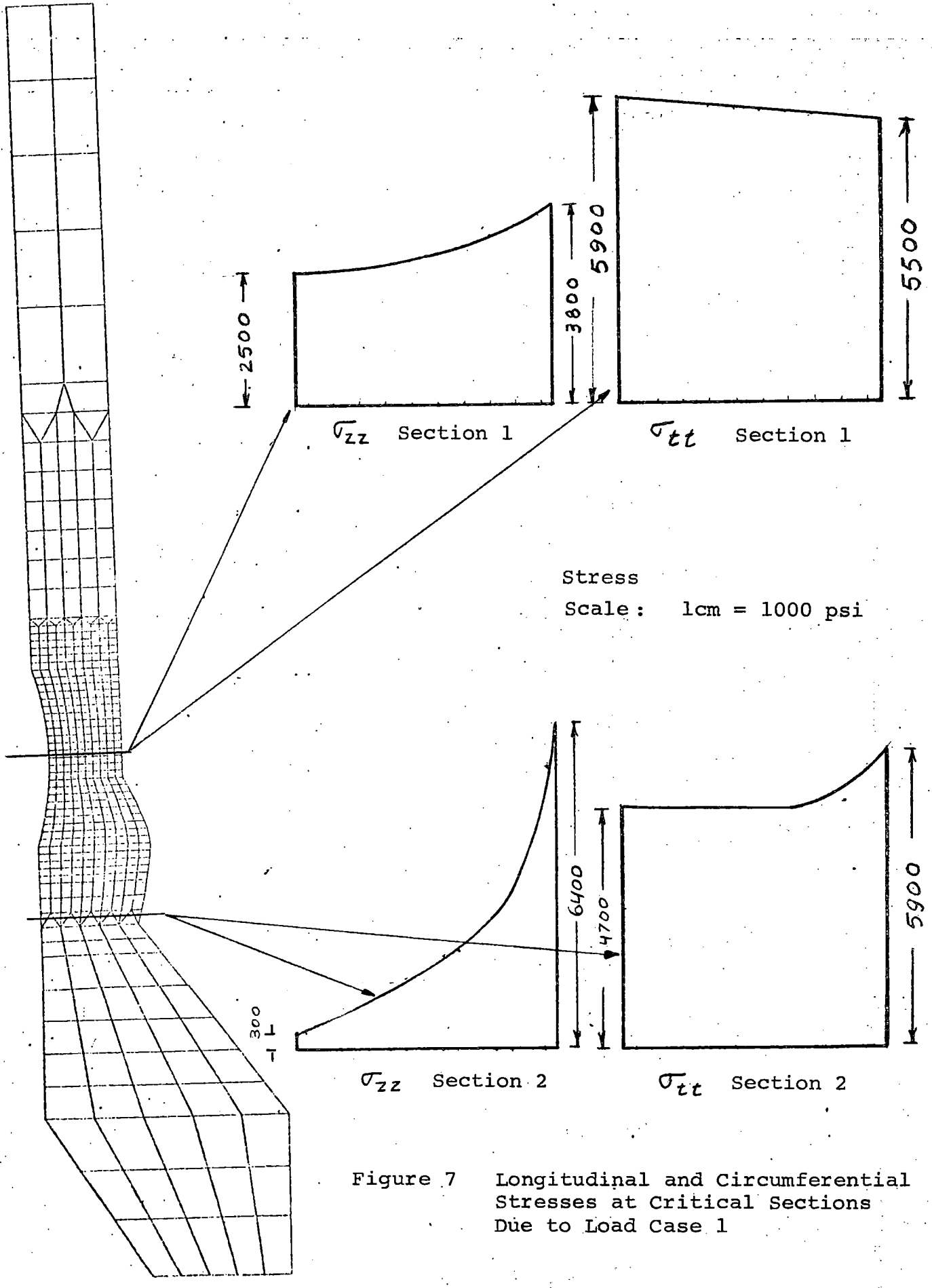

Figure 7 Longitudinal and Circumferential Stresses at Critical Sections Due to Load Case 1

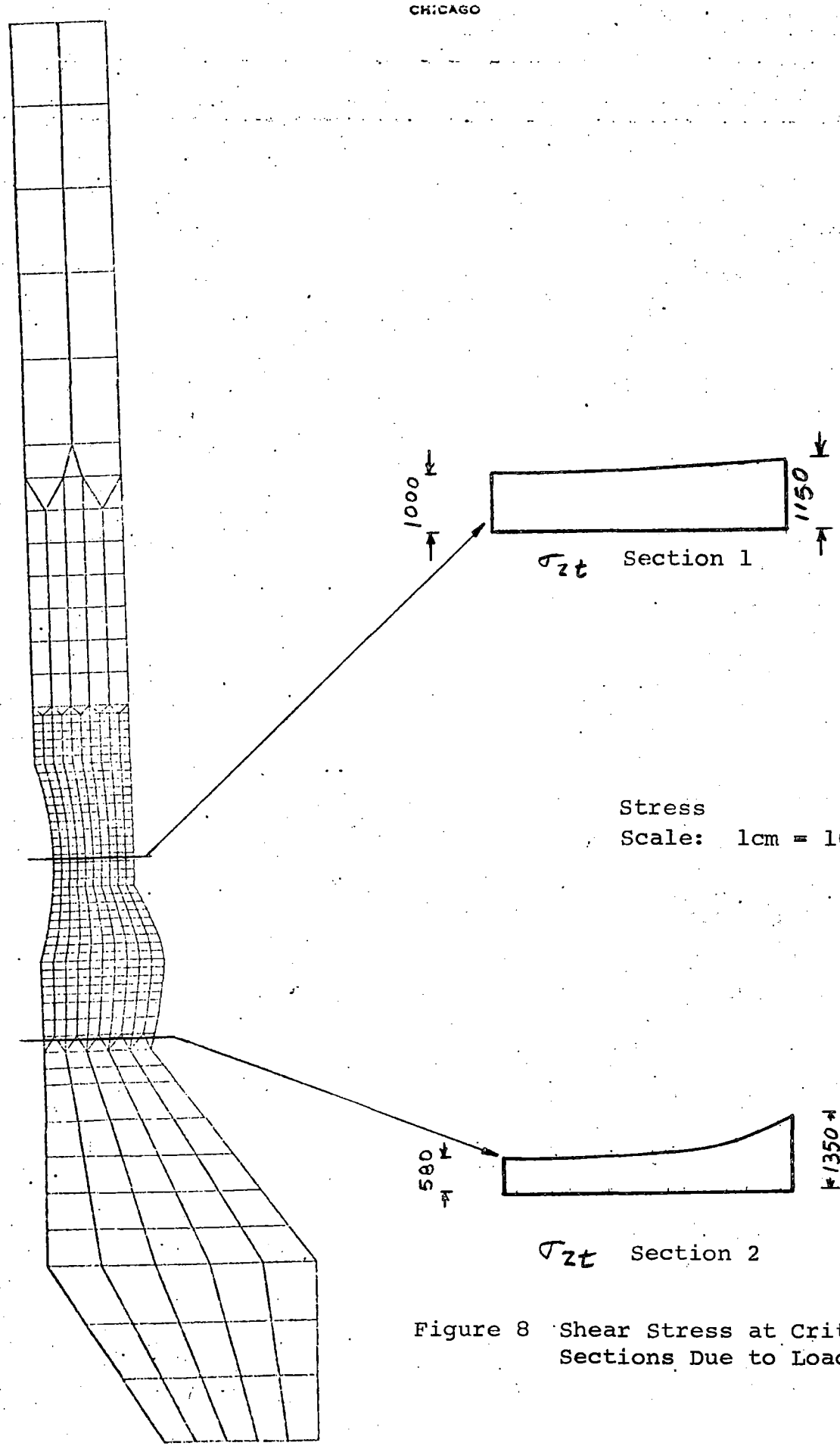

Figure 8 Shear Stress at Critical Sections Due to Load Case 2

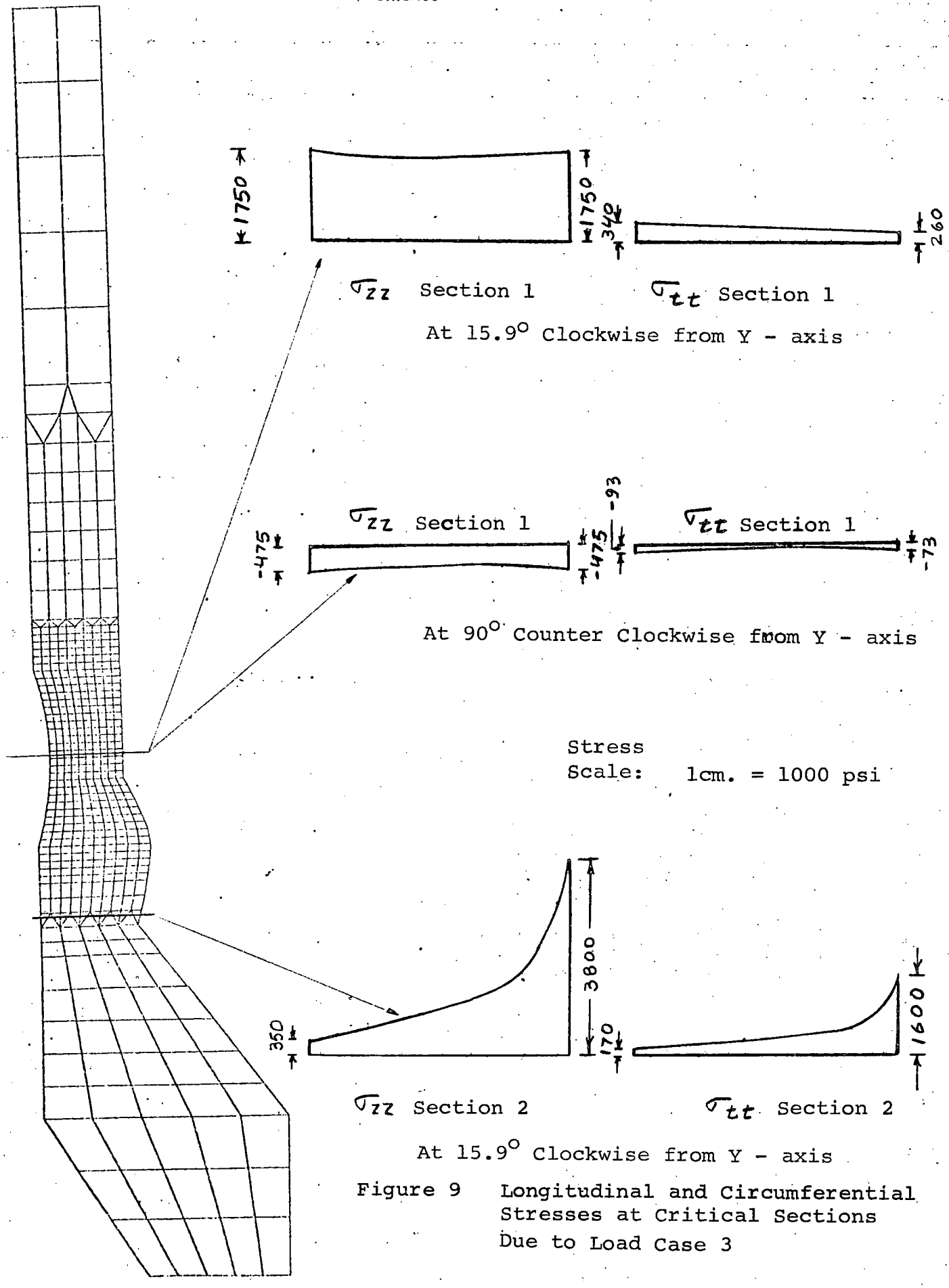

Figure 9 Longitudinal and Circumferential Stresses at Critical Sections Due to Load Case 3

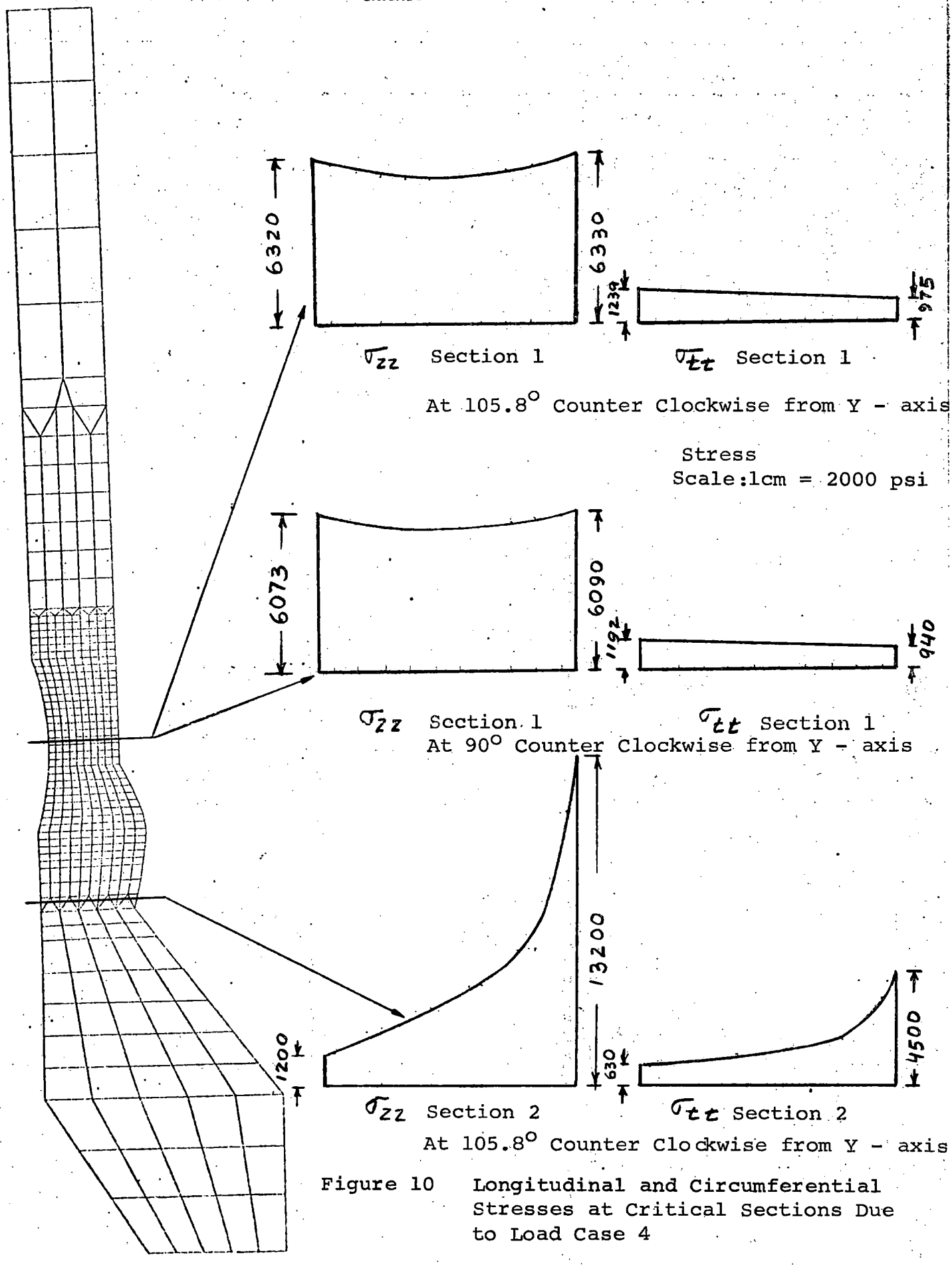

Figure 10 Longitudinal and Circumferential Stresses at Critical Sections Due to Load Case 4

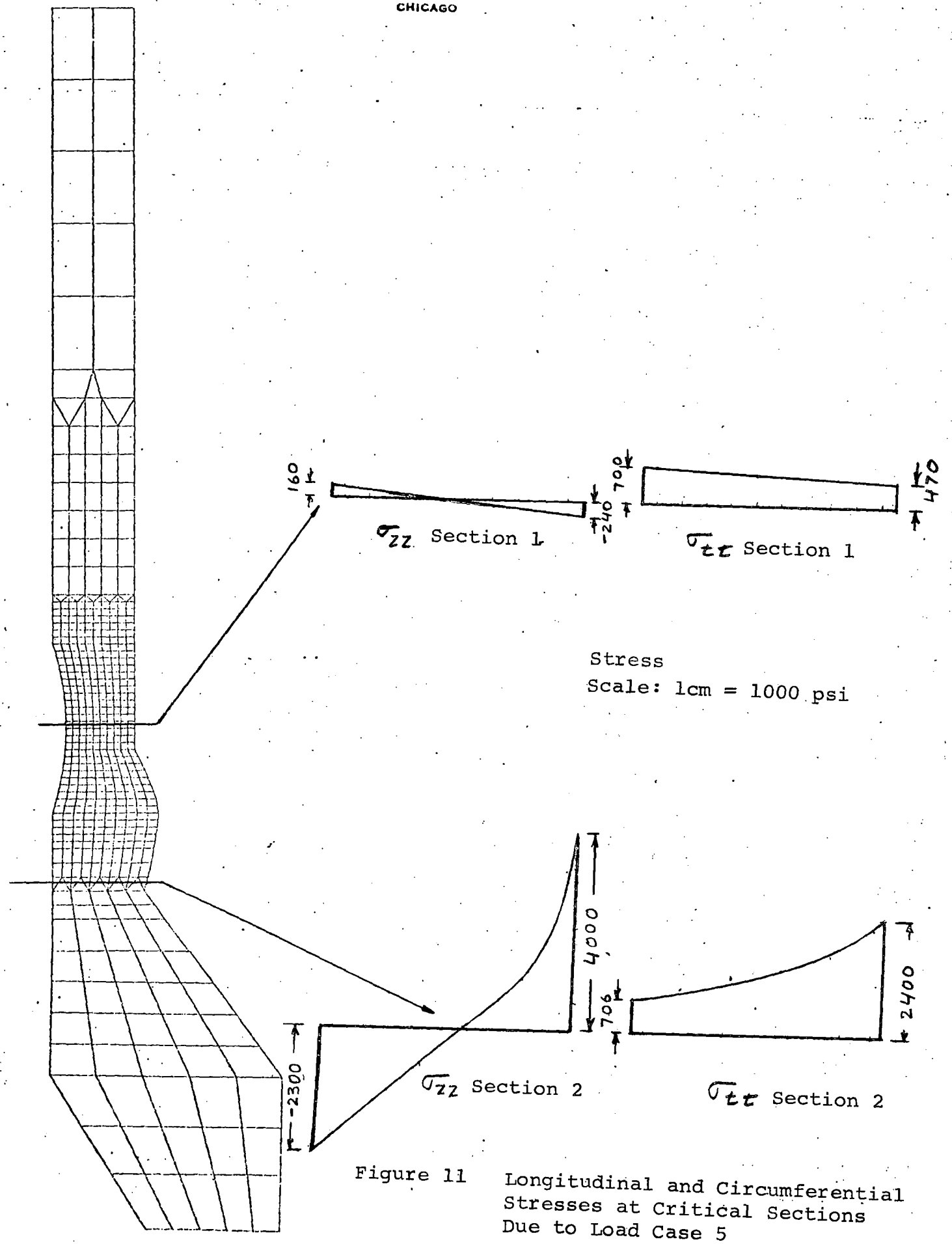

Figure 11 Longitudinal and Circumferential Stresses at Critical Sections Due to Load Case 5

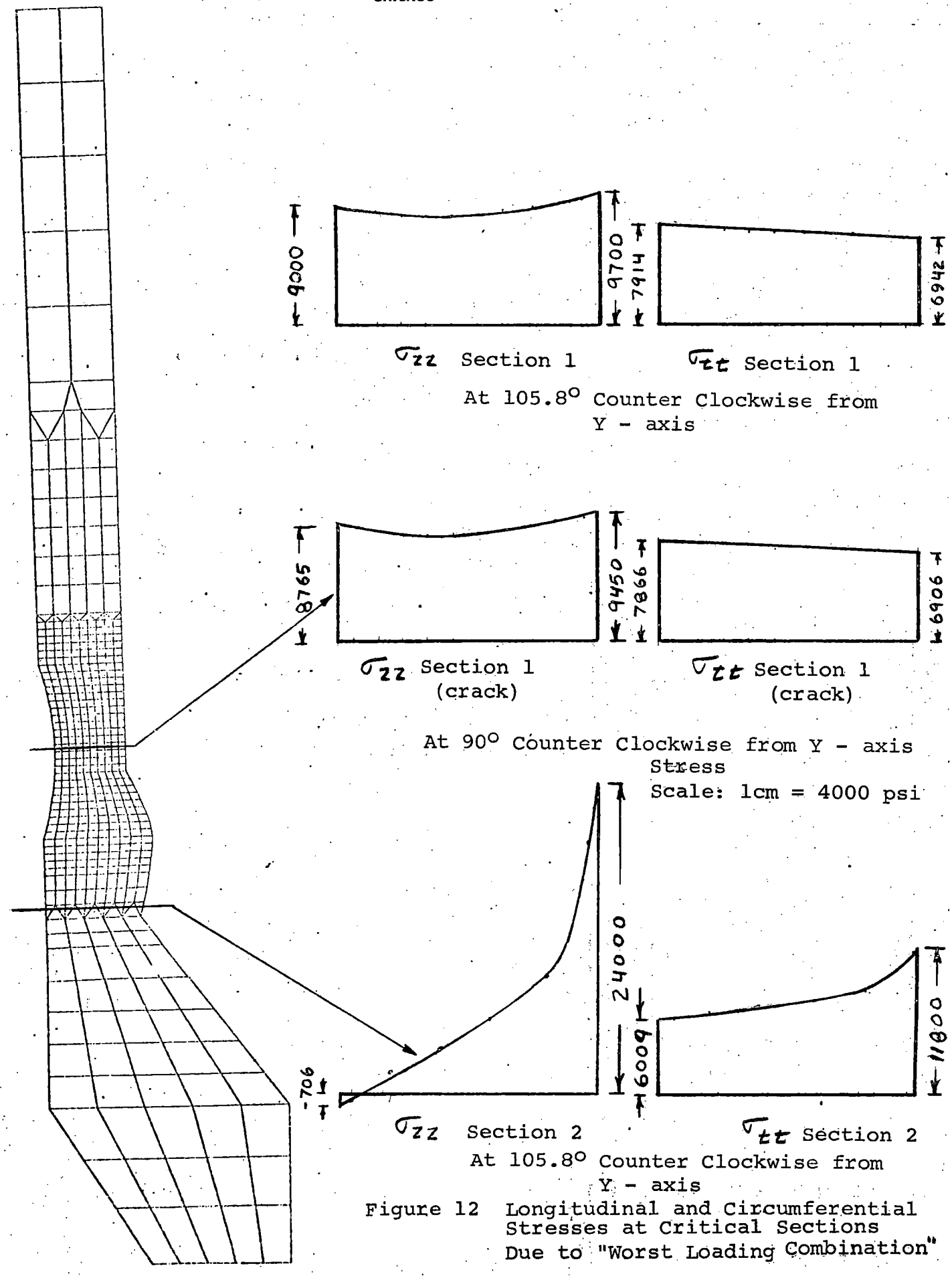

Figure 12 Longitudinal and Circumferential Stresses at Critical Sections Due to "Worst Loading Combination"

APPENDIX A

REFERENCES

1. Timoshenko, S., and Woinowski-Krieger, S., "Theory of Plates and Shells," McGraw-Hill, New York, 1959.

2. Dunham, R. S., Nickell, R. E., "Report Number 67-6 Finite Element Analysis of Axisymmetric Solids with Arbitrary Loadings," Structure Engineering Laboratory, University of California, Berkeley, California, June 1967.

3. "ASM Metals Handbook," Vol. 1, 8th Edition.

4. Farhoomand, I., Wilson, E. L., "Non-Linear Heat Transfer Analysis of Axisymmetric Solids," Structural Engineering Laboratory," University of California, Berkeley, California, April 1971.